Agricultural and Forest Meteorology 198–199 (2014) 53–61

Contents lists available at ScienceDirect

Agricultural and Forest Meteorology

journal homepage: www.elsevier.com/locate/agrformet

Wind and plume thermodynamic structures during low-intensity subcanopy fires

Daisuke Seto[a,*], Tara M. Strand[b], Craig B. Clements[a], Harold Thistle[c], Robert Mickler[d]

[a] Fire Weather Research Laboratory, Department of Meteorology and Climate Science, San José State University, San José, CA 95192, USA
[b] Scion New Zealand Crown Research Institute, Christchurch, NZ 8041, USA
[c] Forest Health Technology Enterprise Team, USDA Forest Service, Morgantown, WV 6505, USA
[d] Alion Science and Technology, Durham, NC 27713, USA

ARTICLE INFO

Article history:
Received 28 January 2014
Received in revised form 26 June 2014
Accepted 16 July 2014

Keywords:
Canopy flow
Fire–atmosphere interactions
Heat flux
Low-intensity fire
Plume rise
Prescribed fire

ABSTRACT

This paper presents observational results of wind and plume thermodynamic structures measured during low-intensity subcanopy fires. In-situ meteorological data were collected during the two experiments in the Calloway Forest in North Carolina during the early spring 2010 and winter 2011. Plume updraft velocities between 2 and 4 m s^{-1} were mostly observed during the subcanopy fires with fire intensity of 1200–2500 kW m^{-1}. A maximum updraft velocity of 5.8 m s^{-1} and maximum temperature of 100 °C were recorded at the canopy top due to a head fire. Negative vertical velocities observed within the canopy were associated with cooler air temperatures relative to warm smoke plume temperatures during fire passage at the towers. Increased convection due to the head fire resulted in increased downward transport from above the canopy to the surface. Observed cumulative sensible heat fluxes were 52 kW m^{-2} and 169 kW m^{-2} near the surface, and larger values were found at mid canopy heights at both towers. The peak total heat flux of 50 kW m^{-2} and peak radiative heat flux of 18 kW m^{-2} observed in 2010 were associated with a head fire moving toward the sensors, whereas lower values of 19 kW m^{-2} and 9 kW m^{-2} were measured at the tower in 2011 as a result of a backing fire moving away from the sensors.

1. Introduction

Moderate to high intensity nature of forest, grassland, and shrubland fires present great concerns for human hazard, economical loss, and community safety in the wildland–urban interface (Mell et al., 2010; Morvan, 2011). In contrast, less threatening low-intensity subcanopy fires common in small prescription burns, such as those conducted in the southern United States, pose a greater concern for local and regional air quality. Because reduced air quality has significant impact on human health, aesthetic visibility, and transportation over a broad range of spatial and temporal scales, smoke from prescribed agricultural and forest burning has been a major research topic in many countries around the world (Goodrick et al., 2012).

Wind under a forested environment is highly variable, and the presence of fire in the forest further complicates the flow. Heilman et al. (2014) suggest that impact of forest on atmospheric flow and the resulting vertical and horizontal dispersion of wildfire smoke emission may be significant in the lower atmospheric boundary layer. There have been a handful of field measurements documenting in-forest winds including Sullivan and Knight (2001) and Taylor et al. (2004). The focus of these two studies was mainly on larger scale wind variability and the field trials were not designed for fine-scale flow measurements at the fire front. Better understanding of low-intensity subcanopy fire dynamics is necessary to improve current and newly-developed models related to wildfire and prescribed burning smoke plume transport and dispersion.

Plume rise and dispersion models are much improved when more detailed information on fire location, rate of spread, and heat are given to the models. For example, Daysmoke (Achtemeier et al., 2011), designed for the simulation of smoke plumes from fires, requires initial vertical velocity and temperature anomaly as well as effective plume diameter. A recent development of a simple three-dimensional model by Strand et al. (2009), originally designed to simulate pheromone concentrations and transport in a forested environment, potentially allows for prediction of near-source smoke concentrations under different forest canopies. If the model can be used to simulate near-source smoke plume behavior and dispersion in the forest canopy, in-situ wind velocity data

* Corresponding author. Tel.: +1 408 924 5189; fax: +1 408 924 5191.
E-mail address: daisuke.seto@sjsu.edu (D. Seto).

http://dx.doi.org/10.1016/j.agrformet.2014.07.006
0168-1923/

collected near the heat source (i.e., fire) are necessary to test the performance and reliability of this model. More recently, Heilman et al. (2013) conducted two comprehensive field measurements during low-intensity prescribed fires in forested environments in order to evaluate the capability of existing coupled meteorological-atmosphere dispersion models to adequately resolve small-scale fire-atmosphere and forest interactions. Such observational data can be used to improve our understanding of fundamental fire-atmosphere-canopy interactions that govern fire and smoke plume behavior. Additionally, recent advances in fire-atmosphere coupled models make it possible to resolve small-scale turbulence and fire-atmosphere interactions. In fact, some of the fire–atmosphere coupled models have shown successful reproductions of wind and thermodynamic structures, necessary for smoke plume modeling, observed during a grass fire experiment (Filippi et al., 2013; Kochanski et al., 2013). To date; however, these models and other fire-atmosphere coupled models (e.g. Linn et al., 2010; Coen et al., 2013) have not been used to simulate subcanopy fires and a suite of observational datasets and knowledge regarding fire-atmosphere and canopy interactions are needed to evaluate these and future models. Accurate numerical simulations require realistic heat input values to set up initial conditions, and those values should ideally be obtained through field experiments or numerical results validated in similar conditions.

Both coupled fire-atmospheric and smoke dispersion models benefit from detailed knowledge in fire-induced heat fluxes. Convective and radiative heat fluxes are not only the two main mechanisms for heat transfer that controls fire spread (Butler et al., 2004; Morandini et al., 2006; Silvani and Morandini, 2009; Cruz et al., 2011) but are a direct indication of the fire's intensity. Frankman et al. (2012) measured the convective and radiant heat fluxes from 13 wildfires including surface fires over pine needle fuel. Their results showed the peak radiant heat flux values of 18–77 kW m^{-2} while peak convective heat flux values ranged from 13 and 140 kW m^{-2}. Silvani and Morandini (2009) showed peak radiant and total heat fluxes of 25 and 40 kW m^{-2}, respectively, over pine needle fuel. Because there is a wide range of the observed heat flux values due to various measurement platforms, further investigation is worthwhile to characterize the heat fluxes based on flame height, fire intensity, or flame geometry. These heat flux values measured under specific wind conditions and in various fuel types in the field are needed for evaluating numerical simulations and improving smoke plume dispersion models (Linn et al., 2010).

Surface sensible heat flux released from the fire also determines the final height that the plume reaches. Sensible heat flux measurements during experimental fires are far more uncommon than convective and radiative heat fluxes, but it is an important parameter in model simulations for representing a fireline as a line source of heat (e.g. Sun et al., 2006; Heilman et al., 2013). Clements et al. (2007) measured the sensible heat flux emitted by a grass fire, which was allowed to burn under the flux tower, and Jenkins et al. (2001) provided estimates of typical sensible heat flux values emitted by a forest fire. Clark et al. (1999) and Coen et al. (2004) measured the sensible heat flux from forest fires using infrared video camera imagery and image flow analysis scheme. While these measurements provided realistic sensible heat flux values that can be used to represent heat output above a wildfire fireline in numerical simulations, these values are from much higher intensity fires than the lower intensity surface fires, suggesting limited usefulness in simulating subcanopy fires. Realistic surface heat flux values are necessary to represent low-intensity fires and subsequent smoke plume transport. Additionally, remote sensing measurements of radiative and/or convective heat from wildfires such as Riggan et al. (2004) provided useful information for simulating plume rise (Freitas et al., 2007; Sofiev et al., 2012), and in-situ heat flux measurements serve necessary data for validating the measurements from above.

The objective of this paper is to present observational results of wind and smoke plume thermodynamic structures measured during low-intensity subcanopy fires. Two in-situ wind and temperature datasets were collected from two prescribed burns that took place in southeastern United States in a longleaf pine forest. These datasets were used to compare winds and plume temperatures for a better understanding of fire and plume behavior similarities and differences in the same forest environment. Total, radiative, and sensible heat fluxes are also discussed to provide some quantitative insight into prescribed fires in forested environment.

2. Field experiment description

2.1. Site and fuel description

Two low-intensity prescribed burns took place on 7 March 2010 and 16 February 2011 at The Nature Conservancy's (TNC) Calloway Forest/Sandhills Preserve in North Carolina, USA (Fig. 1). The experimental burns were surface fires under a longleaf pine canopy (*Pinus palustris* Mill.) sitting on gently rolling terrain of old sand dunes. TNC restores this forest by using prescribed fires to mimic the natural fire-return interval, reduce fuels, and to build a healthy habitat for the endangered red-cockaded woodpeckers. The mean tree height (h_c) was 20 m. The soil was sandy with little to no organic matter beyond the surface duff layer. The surface fuels consisted of longleaf pine litter, both cured and live wiregrass (*Aristida stricta*), American turkey oak (*Quercus laevis*), gallberry (*Ilex glabra*), and regeneration longleaf pine. Although small dead tree stems and branches were present on the ground, they were very few and did not carry the fire. Pre-burn fuel loadings in Burn 1 (2010) and Burn 2 (2011) were 0.78 kg m^{-2} and 1.44 kg m^{-2}, respectively. The managed fire-return intervals over the previous ten years were 2 years on average for Burn 1 and 3 years for Burn 2. The stand density for Burns 1 and 2 was 203 stems ha^{-1} and 348 stems ha^{-1}, respectively. A majority of the stems were approximately 1 m mean diameter at breast height (dbh). Further site and fuel information is summarized in Table 1.

2.2. Weather

Background weather observations were made using upper-air rawinsondes for determining stability and local vertical wind profiles. The rawinsonde sounding was conducted in a large clearing near the burns prior to ignition. For Burn 1, winds were westerly and <5 m s^{-1} up to 1 km above ground level (AGL), while for Burn 2 winds were from southeast to southwest and mostly <10 m s^{-1} from the surface to 1 km AGL (Fig. 2). The mixing height was around 1.5 km AGL for Burn 1 and 1 km AGL for Burn 2, as indicated by a capping temperature inversion and sharp drop in the dewpoint temperature. The atmospheric stability below the mixing height was neutral to weakly stable except near-surface where an unstable superadiabatic layer was observed. A relative humidity of 20% was observed at the tower before ignition of Burn 1 and it ranged from 13% and 18% during the burn. For Burn 2 the relative humidity prior to ignition was 30% and it remained between 35% and 40% throughout the duration of the burn.

2.3. Fire

The burn manager and interior ignition crews controlled the fire by slowing down the interior ignition to cool down the fire when necessary. It kept the flame height relatively low to prevent canopy scorch. Initial backing fires (fire moving against predominant wind

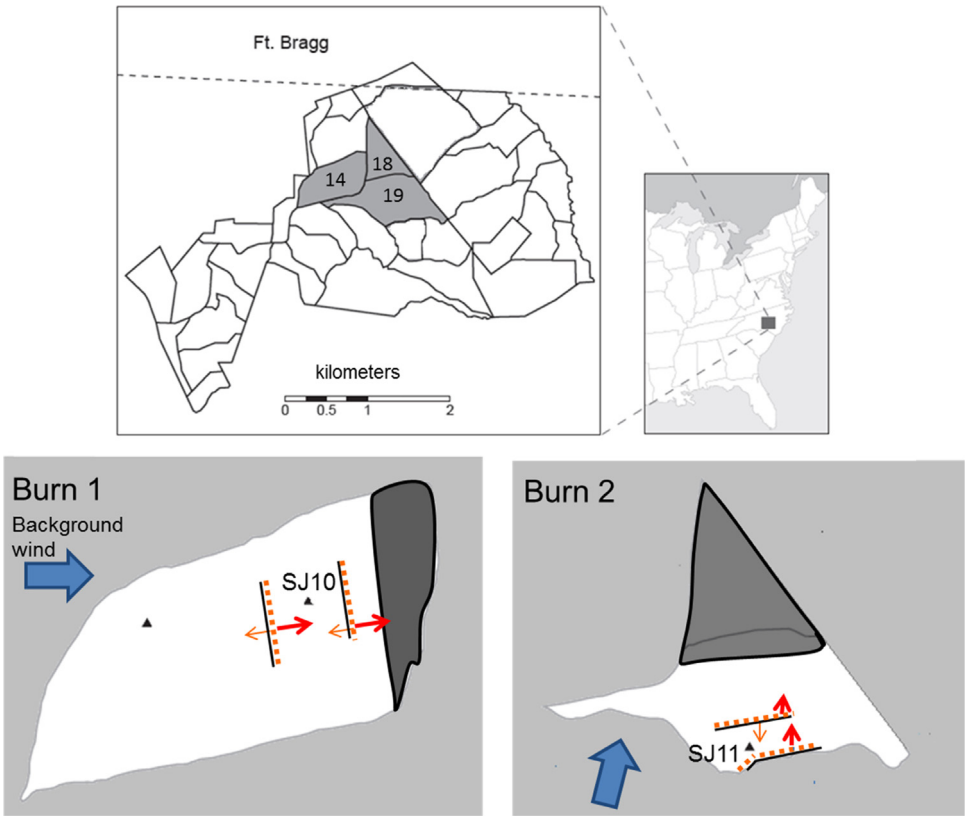

Fig. 1. A map of experimental site showing Burns 1 and 2 and instrument tower locations (SJ10 and SJ11). Firelines are shown with orange dotted lines to give a general idea of the interior ignition pattern near the tower and types of fire. Direction of head fire (red arrow) and backing fire (orange arrow) are shown. Shaded areas indicate burnt fuel. Background wind directions are also shown in large blue arrows. Blackline ignitions are not shown here but can be seen in Figs. 3 and 4. (For interpretation of the references to color in this figure legend, the reader is referred to the web version of this article.)

Table 1
Burn and fuel information including the flux tower names. Fuel moisture values are averaged across all fuel beds.

Tower	Burn date	Latitude Longitude	Size (km^2)	Start of hand ignition (EST)	End of hand ignition (EST)	Fule load		Fuel moisture content (%)	Maximum flame height (m AGL)
						Pre-burn ($kg\,m^{-2}$)	Post-fire ($kg\,m^{-2}$)		
SJ10	7 Mar 2010	35.2333N, 79.369W	0.25	11:20	15:20	0.78	0.21	35	11
SJ11	16 Feb 2011	35.6360N, 79.5038W	0.71	11:00	17:00	1.44	0.21	38	2

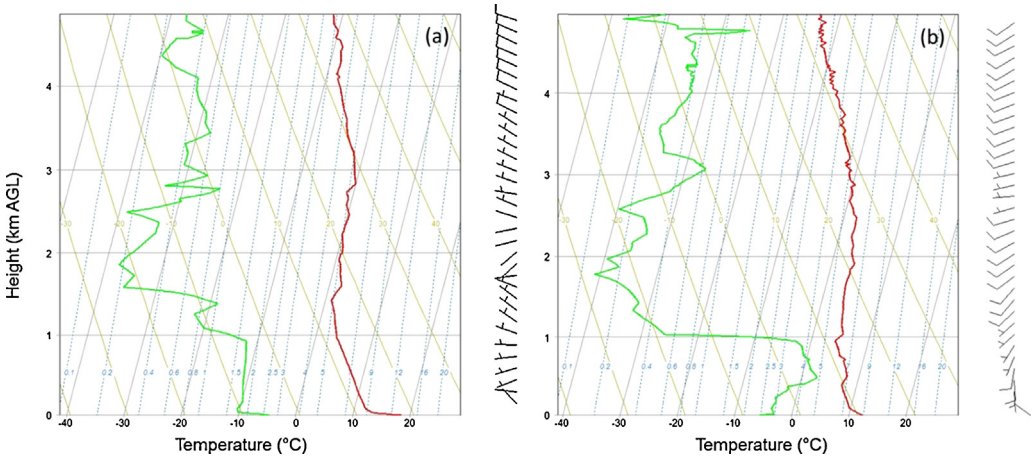

Fig. 2. Sounding profiles of temperature (red), dew point (green), and wind speeds and directions plotted with height observed prior to the ignition; (a) at 11:20 EST on 7 Mar 2010, (b) 11:18 EST on 16 Feb 2011. Lines of dry adiabat (light brown lines), and saturation mixing ratio (blue dash lines) are also shown in the background. Statically stable (unstable) layers are where the temperature line is steeper (less steep) than the nearest dry adiabats, and neutral layers are where the two lines are parallel. (For interpretation of the references to color in this figure legend, the reader is referred to the web version of this article.)

Fig. 3. Photographs showing (a) SJ10 tower, heat flux sensor box in front of the tower, and blackline ignited downwind side of the tower; (b) a line of strip head fire ignited upwind of the tower; (c) and (d) flames engulfing the tower and heat flux sensors.

direction) at the downwind corner of the burn unit and along the burn perimeter were followed by strip and spot head fires (fire moving with predominant wind direction) ignited by interior fire crews. For both towers, the downwind side of the tower was first ignited (backing fire) before a head fire was ignited on the upwind side (Fig. 1).

Rate of fire spread was measured in Burn 2 by placing a transect of 1 m aluminum poles perpendicular to the ignition lines, and then the fire propagation was recorded via video by an interior igniter. The rate of fire spread was calculated using the known distance between the poles and the time it took for the head fire to reach the pole. Maximum flame height was also estimated with video and the poles, which were painted black and white alternately every 0.3 m (Table 1).

In this paper, blackline refers to a burning technique used by the hand igniters during the experimental burns to create a safe fire perimeter and to protect the endangered red cockaded woodpeckers' nesting trees and the research towers. The technique surrounded the instrument towers with a small amount of consumed fuel ('blackline'), which reduced the heat intensity directly near the instrument. For Burn 1, fire was allowed to approach the instrumented tower after the downwind side of the tower was blacklined (Fig. 3). Given the conditions of the day the tower base was fully blacklined during Burn 2 (Fig. 4).

3. Instrumentation and data processing

3.1. Instrumentation

A 20 m guyed aluminum tower, deployed within each burn unit was equipped with instrumentation that measured wind and temperature structures. Hereafter, we refer to these towers as SJ10 (Burn 1) and SJ11 (Burn 2). The SJ10 was located in the middle of Burn 1 and the SJ11 was located in the interior but near the southern edge of Burn 2 (Fig. 1). Both towers were equipped with three 3-dimensional sonic anemometers. Two (Sx-probes, Applied Technologies, Inc., Colorado, USA) were custom-calibrated beyond 100 °C and placed at 3 m and 10 m AGL and one sonic anemometer (Model 81000, R. M. Young Company, Michigan, USA) calibrated up to 50 °C was mounted at 20-m AGL. The sonic anemometers recorded winds at 10 Hz.

A type-T fine-wire thermocouple (5SC-TT-T-40, Omega, Inc., Connecticut, USA) was placed every meter from the ground up to 20 m AGL to measure plume temperature profiles. Because small wire and bead size reduce losses or gain due to radiant energy transfer and also decrease thermocouple response time (Butler et al., 2004), the 40 American Wire Gauge (AWG) size thermocouples (0.076 mm diameter at bead) were used to minimize the effect of radiation on thermocouple temperature measurements near the flame. The thermocouple data were sampled at 10 Hz and saved to 5 Hz. Clements (2010) has shown successful measurement of plume thermodynamic structure during a grass fire experiment using the same thermocouple diameter.

Additionally, total and radiative heat fluxes were measured at both tower sites using a Schmidt–Boelter gauge total heat flux sensor (Hukseflux, SBG01, Delft, The Netherland) and a Gardon gauge radiant heat flux sensor (Medtherm, 64P-50-24, Alabama, USA), respectively. These sensors are widely used in fire research and in fire testing laboratories to measure heat flux (Pitts et al., 2006). The Hukseflux total heat flux and the Medtherm radiative heat flux sensors have 180 and 150° field of view, respectively. The heat flux sensors were mounted in a rectangular aluminum box, and the sensor box was attached to a fence post placed approximately 3 m from the tower. A temperature and humidity sensor (HMP45C, Campbell Scientific Inc., Utah, USA) was mounted on the tower at 3 m AGL to monitor in-canopy atmospheric conditions. Both the tower base and heat flux sensor box were protected from the extreme heat of the fire using fireproof insulation material. To prevent flames from

Fig. 4. Photographs showing SJ11 tower, heat flux sensor box (indicated with a red arrow), blackline ignited around the tower, and backing fire approaching to the tower. (For interpretation of the references to color in this figure legend, the reader is referred to the web version of this article.)

touching the tower base, fuel immediately around the base was removed.

3.2. Data processing

Daytime data between 09:00 to 17:00 USA Eastern Standard Time (EST) on the day of the experimental fires were used in the analyses. Time series data from the sonic anemometers were first inspected visually to remove unrealistic spikes. A despiking routine (Vickers and Mahrt, 1997) was performed to remove erroneous spikes. During high temperature environment associated with a fire passage, data larger than four times the standard deviation within a 1 min moving window were replaced by linearly interpolated values. We chose ±4 standard deviations for the lower intensity nature of our burns, based on Clark et al. (1999) and Coen et al. (2004) who suggested ±5 standard deviations from the mean wind velocity as plausible estimate of fire-induced wind extremes. The vertical velocity component, w, was tilt-corrected following Wilczak et al. (2001). To calculate sensible heat flux, the sonic temperature and vertical velocity perturbations, T_s' and w', respectively, were calculated by using their 30 min mean values. In the high temperature fire periods, the mean values prior to the fire front passage at each tower were used to represent the undisturbed background atmosphere. The sensible heat flux was averaged over 1 min. Timing of fire front passage at the tower was determined from the data and verified with photos as much as possible.

4. Results and discussion

4.1. Wind velocities and smoke plume temperatures

In this section, 1 s averaged in-plume wind velocity and temperature data were used to investigate the thermal structure of the smoke plume and associated wind motions above the fire. For Burn 1, a blackline was ignited on the downwind side of the SJ10 tower base at 12:52 EST (Fig. 3a). At the same time, fuel approximately 30 m upwind of the tower was ignited to allow for a head fire to move toward the tower (Fig. 3b). Photography images indicate that a maximum flame height near the tower was approximately 1 m AGL.

The first notable temperature rise was measured at 12:58 EST with a maximum thermocouple temperature of 54 °C near the surface (Fig. 5a), and this was associated with a backing fire passing on the right side of the tower (Figs. 3b). Another high thermocouple temperature of 78 °C was observed around 13:00 EST near the surface, and it occurred when a head fire ignited upwind of the tower converged with the slow moving backing fire on the upwind side of the tower (Fig. 3d). The peak updraft velocities associated with the fire passage were 2–4 m s^{-1} with the strongest updrafts measured at z = 0.5 h (Fig. 5b). Intermittent negative vertical velocities observed mainly at z = 0.15 h and 0.5 h were associated with cool ambient air in the canopy space (e.g. 12:59, 13:06, and between 13:11 and 13:13 EST in Fig. 6a and b), which likely originated from above the canopy.

Fig. 4a shows a blackline ignition around the SJ11 tower in Burn 2. In contrast to Burn 1, the blackline was ignited around the entire tower base. The approaching backing fire is visible behind the tower in Fig. 4b. The backing fire reached the tower around 16:04 EST (Fig. 4c). A head fire ignited upwind of the tower reached near the tower at 16:16 EST as measured radiative heat flux, discussed in the next section, suggests the presence of flame nearby the sensor. The flame heights near the tower were approximately 1 m AGL but locally reached up to 2 m AGL.

A maximum temperature of 147 °C at 1 m AGL at 15:58 EST was associated with blackline ignition around the tower (Fig. 6). Higher Fuel loadings in Burn 2 likely resulted in the higher near-surface plume temperatures. Despite the higher temperatures during fire front passage, this blackline caused similar updraft vertical velocities between 3 and 4 m s^{-1} at $z = 0.15\,h$ to those observed during Burn 1. The arrival of the backing fire at the tower after the blackline was accompanied with similar peak plume updraft velocities between 3.0 and 3.5 m s^{-1} observed at z = 0.5 h and 1.0 h. Smoke plume temperatures measured between 16:16 and 16:19 EST were as high as 100 °C at the canopy top, with a maximum updraft velocity of 5.8 m s^{-1} at this height (Fig. 6b). The topmost sonic anemometer was only calibrated up to 50 °C, but data inspection revealed few erroneous spikes in the wind velocity in relation to the high sonic temperatures, and a thermocouple temperature at the same height measured nearly the same magnitude. Therefore, we believe this to be a good value. Increased negative vertical velocities at z = 0.15 h and 0.5 h were noticeable within the smoke plume, similar to the observations made at the SJ10.

The relationships between the observed plume temperatures and associated vertical velocity motions are better illustrated by their scatter plots in Fig. 7. While larger T_s' were observed at the SJ10 tower at z = 0.15 h than those observed at the SJ11, similar T_s' vs. w scatter patterns were evident between the two towers during the fire front passage, regardless of the difference in types of fire, heading (SJ10: 12:57–13:02 EST) or backing (SJ11: 16:03–16:08 EST). Low-intensity subcanopy fires may enhance the downward motions within the canopy in response to fire-induced updrafts. Often in forests, weak ejection motions of warm air transported out of the forest are followed by strong sweeping motions of cool air into the canopy (Gao et al., 1989). The observed strong downward motions between 16:16 and 16:18 EST also increased horizontal wind speeds within the canopy. It indicates that the downward transport of momentum from above the canopy to the surface occurred as a result of stronger convection associated with the head fire on the upwind of the tower. Similar enhanced downward momentum transport has been observed during an open grass fire environment (Clements et al., 2007) and in simulations by Sun et al. (2009). Fire intensity was approximately 1200 kW m^{-1} during Burn

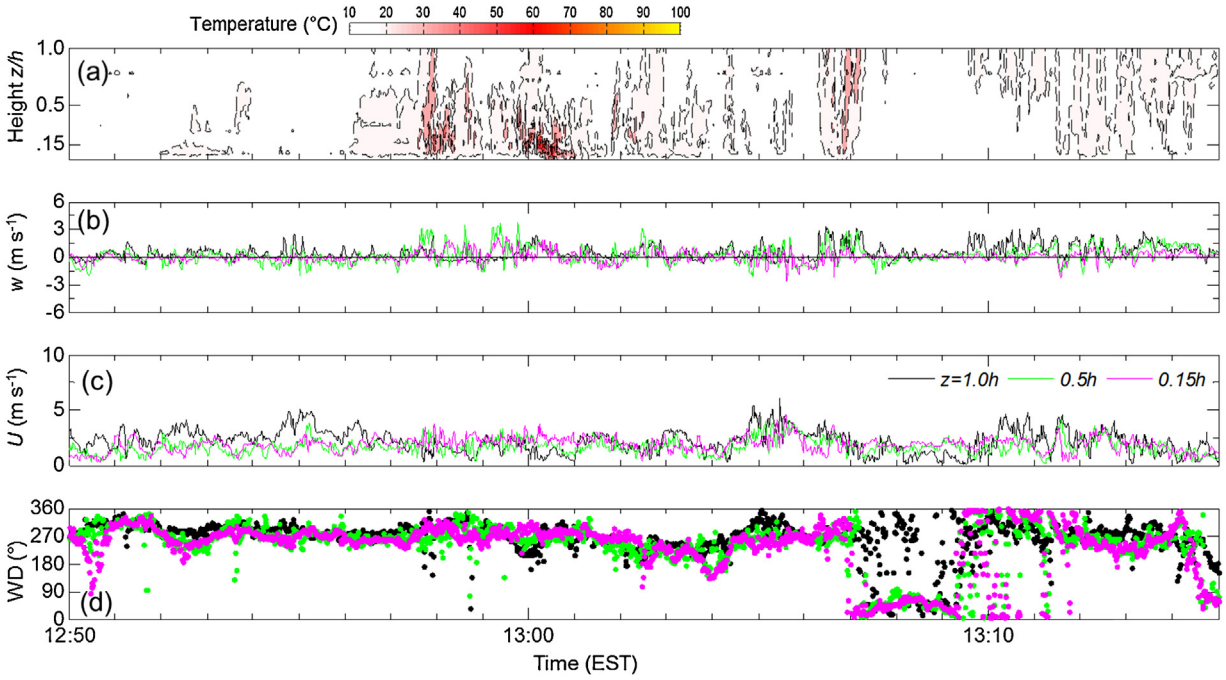

Fig. 5. Time series of 1 s averaged (a) plume temperatures (b) vertical wind velocities, (c) horizontal wind speeds, and (d) wind direction observed at SJ10 tower. Timing of ignition around tower is shown in Fig. 3. The wind measurement heights were $z = 1.0$ h (black), 0.5 h (green), and 0.15 h (purple). (For interpretation of the references to color in this figure legend, the reader is referred to the web version of this article.)

1 using an estimated rate of head fire spread of 0.12 m s^{-1} near the SJ10 tower and measured fuel consumption in Table 1.

Observed average head fire spread rate of 0.14 m s^{-1} suggests that the fire intensity was approximately 2500 kW m^{-1} during Burn 2. The higher fire intensity observed in Burn 2 may have caused the observed strong downward motions. These downward motions may be important to the subcanopy fire behavior because they may carry fresh air that supplies oxygen to the fire along with higher momentum. Consequently, this type of fire-atmosphere interaction may cause rapid increases in fire growth and heat release. Another implication is that the downward motions may be strong enough to transport active turbulence and coherent eddies above the canopy down to the surface fire. The enhanced interactions between the layer below the canopy and the atmospheric layer above the canopy due to the fire will influence the mixing process and dilution of the smoke plume.

The impact of blackline ignition on our temperature profile and wind velocity measurements must be kept in mind when considering these values for smoke plume rise from controlled burns. The measured thermocouple temperatures near the surface during the

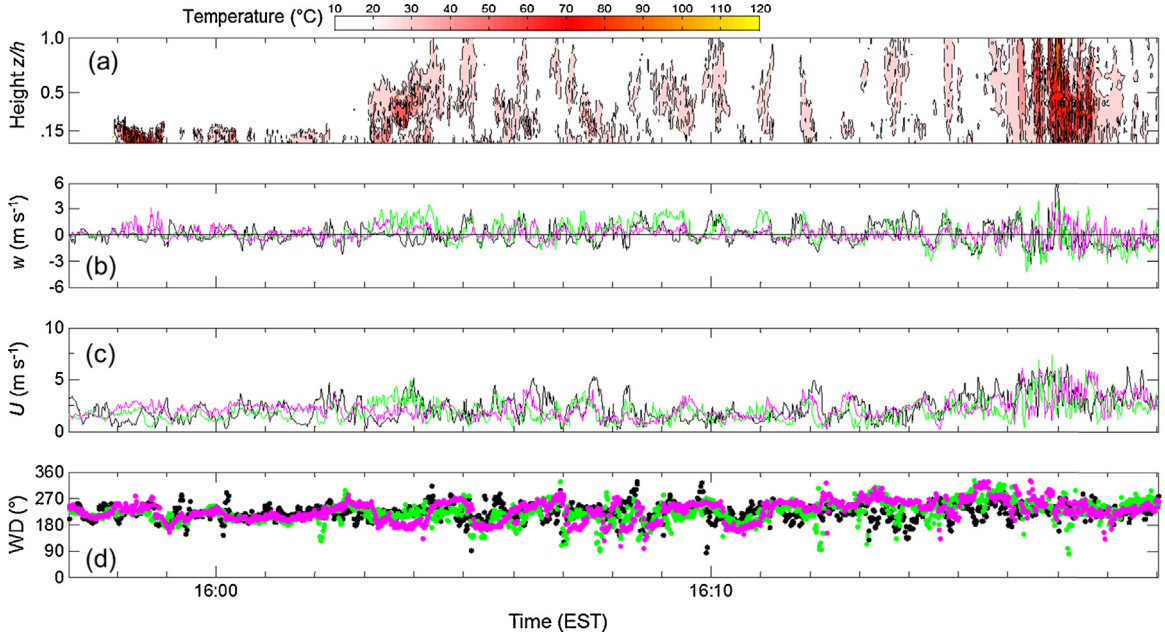

Fig. 6. Time series of 1 s averaged (a) plume temperatures (b) vertical wind velocities, (c) horizontal wind speeds, and (d) wind direction observed at SJ10 tower. The winds were measured at $z = 1.0$ h (black), 0.5 h (green), and 0.15 h (purple). Timing of blackline ignition at the SJ11 tower is shown in Fig. 4. Temperature scale in Fig. 6a is different from Fig. 5a to show higher plume temperatures. (For interpretation of the references to color in this figure legend, the reader is referred to the web version of this article.)

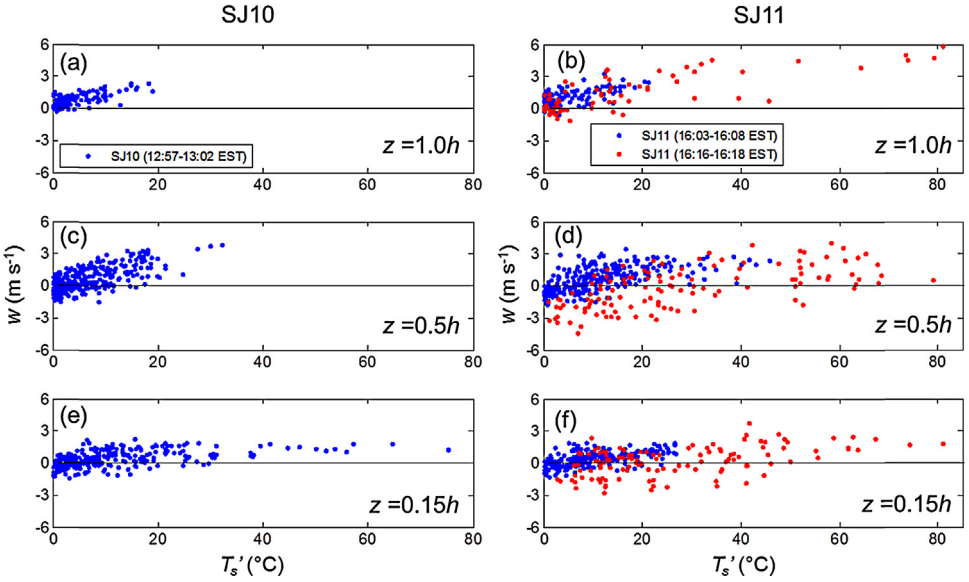

Fig. 7. Scatter plots of 1 s sonic temperature perturbation T_s' vs. vertical velocity w. measured during fire passage (left) at the SJ10 tower between 12:57 and 13:02 EST and (right) at the SJ11 tower between 16:03 and 16:08 EST (blue dots) and between 16:16 and 16:18 EST (red dots). (For interpretation of the references to color in this figure legend, the reader is referred to the web version of this article.)

fire front passage may underestimate plume temperatures near the surface compared to those fires without the blackline. If higher fire intensity is expected due to the absence of blackline, stronger downward motions would promote more effective mixing within the canopy.

4.2. Sensible, total, and radiative heat fluxes

Fig. 8 shows accumulations of sensible heat fluxes H_s associated with the fire passage at each tower. At SJ10, H_s of 52 kW m^{-2}, measured at z = 0.15 h, was emitted into the atmosphere by a head fire passage. In contrast, a cumulative H_s of 169 kW m^{-2} was observed at SJ11 due to the blacklining, backing, and head fires. The blackline ignition and approaching head fire were associated with relatively quick increases in H_s, whereas only the backing fire showed a steady increase in H_s. The cumulative sensible heat flux values measured at z = 0.5 h were 90 kW m^{-2} and 180 kW m^{-2} at the SJ10 and SJ11 towers, respectively, and the values decreased to 66 kW m^{-2} and 119 kW m^{-2} at z = 1.0 h, respectively. The total heat output from subcanopy prescribed fires may be characterized by multiple increases in the sensible heat flux over a relatively long time period due to multiple ignition lines. Non-linear increases in the observed sensible heat fluxes over the time indicate varying maximum plume top heights, which place the smoke plumes into different horizontal wind transport layers between the ground and plume top.

Both towers saw total and radiative heat fluxes peaked at the same time. The observed peak total and radiative heat fluxes were 50 kW m^{-2} and 18 kW m^{-2} in Burn 1 as a head fire moved toward the sensors (Fig. 9). In contrast, the respective heat flux values were 19 kW m^{-2} and 9 kW m^{-2} in Burn 2 as a result of a backing fire moving away from the sensors. The comparatively low heat fluxes in Burn 2, despite a higher fuel loading than Burn 1, were caused by smaller flame depth and lower fire intensity associated with the backing fire. The secondary heat flux peak that coincided with high plume temperatures was associated with a head fire that did not reach the sensor because the fuel ahead of the head fire was already consumed by the backing fire. Most of the sensible, total, and rediative heat fluxes occurred in relatively short period of time in Burn 1 due to the relatively quick moving head fire, while gradual accumulations in the heat fluxes were evident in Burn 2 associated with the slow moving backing fire. Higher fraction of the convective heat flux was also evident with the head fire in Burn 1. Our measurements of the heat fluxes in Burn 1 are similar in magnitude to the peak total heat flux of 40 kW m^{-2} and radiative heat flux of 25 kW m^{-2} observed by Silvani and Morandini (2009) during a fire spread experiment over a pine needle fuel bed. The different fire front geometry in front of the heat flux sensors observed in Burns 1 and 2 made for a direct comparison between their relative magnitudes. The measured total and radiative heat flux values in Burn 1 may be more representative of a low-intensity subcanopy fires. The radiative heat flux is essentially proportional to the fourth power of the temperature of the heat source, so these maximum radiative

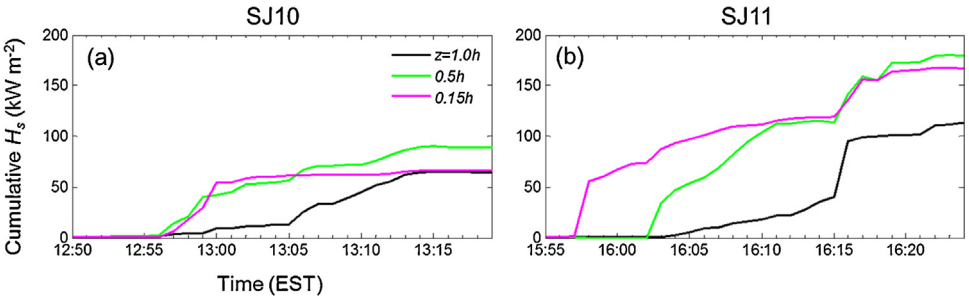

Fig. 8. Time series of 1 min averaged cumulative sensible heat fluxes during the fire passage at (a) SJ10 and (b) SJ11 towers.

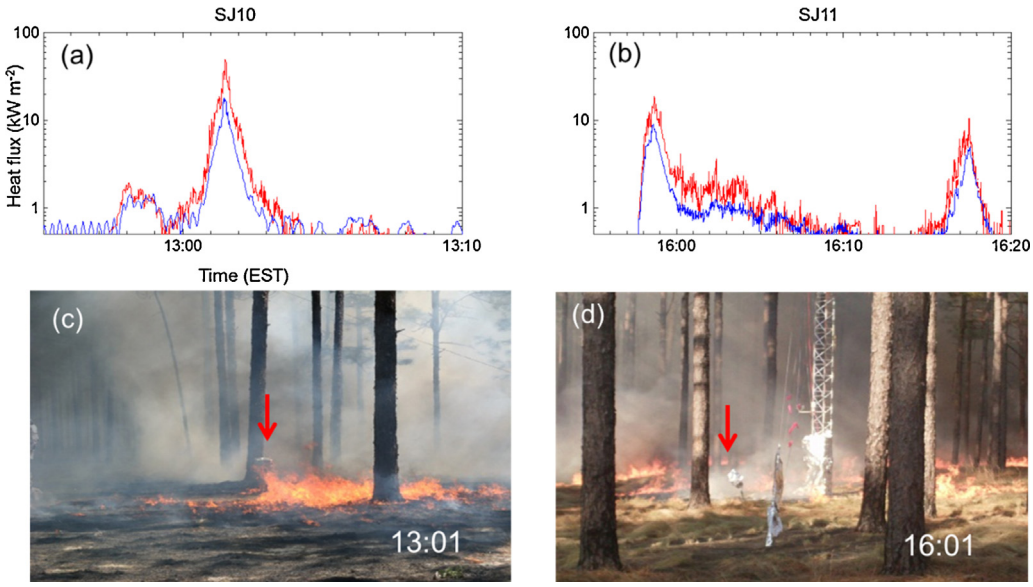

Fig. 9. Time series of 1 Hz total (red) and radiative (blue) heat fluxes measured at (a) SJ10 and (b) SJ11 towers plotted on logarithmic scale. Pictures below show fire front and the heat flux sensor box as indicated by red arrows. (For interpretation of the references to color in this figure legend, the reader is referred to the web version of this article.)

heat fluxes can be used directly to simulate plume rise in the future as suggested by Freitas et al. (2007).

5. Summary and conclusions

This study focused on analyses of in-situ wind and plume thermodynamic during low-intensity surface fires in a fuel bed dominated by pine litter fuel. The two burns took place in the same forest with similar fuel beds, and wind velocity and plume temperature data measured during fire front passage provided insight into the similarity and contrast between the two prescribed fires with different fire types under the flux towers. Some of the key findings from this study are;

(1) In-situ wind velocity data showed 1 Hz plume updraft velocities mostly between 2 and 4 m s^{-1}, represented by a fire intensity that ranged from 1200 to 2500 kW m^{-1}. A maximum updraft velocity of 5.8 m s^{-1} and maximum temperature of 100 °C were measured at the canopy top and this was associated with a head fire (Burn 2).
(2) Downward motions, observed mainly at $z = 0.15$ h and 0.5 h in the subcanopy fire environment, were associated with cooler temperatures. It was found that increased heat output may result in increased downward motions as a result of atmospheric feedback. Increased horizontal velocities were also found with the increased downward motion (Burn2).
(3) The cumulative sensible heat flux values of 52 kW m^{-2} and 169 kW m^{-2} were found near the surface (3 m AGL) at the SJ10 and SJ11 towers, respectively, while the maximum value occurred at mid canopy heights at both towers. Non-linear increases in the observed sensible heat fluxes indicate varying maximum plume top heights. The peak total heat flux of 50 kW m^{-2} and peak radiative heat flux of 18 kW m^{-2} observed at the SJ10 tower were associated with a head fire moving toward the sensors, whereas lower values of 19 kW m^{-2} and 9 kW m^{-2} were measured at the SJ11 tower as a result of a backing fire moving away from the sensors.

Our data are representative of typical subcanopy prescribed fires in which spot and strip head fires are commonly used for ignitions. While the magnitudes of the observed winds, temperatures, and heat fluxes from these prescribed subcanopy fires are relatively small compared to higher intensity wildfires, including these meteorological data collected in the low-intensity fire environment may have significant impact on simulating plume rise and smoke transport. Because our data were measured under daytime condition where the atmosphere promotes productive mixing, different interactions may occur under more stable atmospheric conditions in the early morning or evening hours or under different canopies. Nonetheless, these field observations are an important step toward developing improved or new smoke transport models from low-intensity burns as three dimensional wind velocity and smoke plume temperature data near the fire are hardly available.

Acknowledgements

This project was funded by the Joint Fire Science Program (JFSP 09-1-4-2). We thank The Nature Conservancy (TNC) North Carolina Chapter who put time and effort into assisting us with this project. In particular, we thank burn boss Mike Norris, TNC Fire Manger Margit Bucher, and the TNC fire crew and volunteers. Their support was essential to success of the project. We also give a special thanks to Andy Trent, Scott Gilmour, and Gary Kees from the USFS Forest Health Technology Enterprise Team for help with the installation and operation of our towers and instrumentations.

References

Achtemeier, G.L., Goodrick, S.A., Liu, Y., Garcia-Menendez, F., Hu, Y., Odman, M.T., 2011. Modeling smoke plume-rise and dispersion from Southern United States prescribed burns with Daysmoke. Atmosphere 2 (3), 358–388.
Butler, B.W., Cohen, J., Latham, D.J., Schuette, R.D., Sopko, P., Shannon, K.S., Jimenez, D., Bradshaw, L.S., 2004. Measurements of radiant emissive power and temperatures in crown fires. Can. J. For. Res. 34, 1577–1587.
Clark, T.L., Radke, L., Coen, J., Middleton, D., 1999. Analysis of small-scale convective dynamics in a crown fire using infrared video camera imagery. J. Appl. Meteorol. 38, 1401–1420.
Clements, C.B., 2010. Thermodynamic structure of a grass fire plume. Int. J. Wildland Fire 19, 895–902.
Clements, C.B., Zhong, S., Goodrick, S., Li, J., Bian, X., Potter, B.E., Heilman, W.E., Charney, J.J., Perna, R., Jang, M., Lee, D., Patel, M., Street, S., Aumann, G., 2007. Observing the dynamics of wildland grass fires: FireFlux—a field validation experiment. Bull. Am. Meteorol. Soc. 88 (9), 1369–1382.

Coen, J., Mahalingam, S., Daily, J., 2004. Infrared imagery of crown fire dynamics during FROSTFIRE. J. Appl. Meteorol. 43, 1241–1259.
Coen, J.L., Cameron, M., Michalakes, J., Patton, E.G., Riggan, P.J., Yedinak, K.M., 2013. WRF-fire: coupled weather-wildland fire modeling with the weather research and forecasting model. J. Appl. Meteorol. Climatol. 52, 16–38.
Cruz, M.G., Butler, B.W., Viegas, D.X., Palheiro, P., 2011. Characterization of flame radiosity in shrubland fires. Combus. Flames 158, 1970–1976.
Filippi, J.B., Pialat, X., Clements, C.B., 2013. Assessment of ForeFire/MesoNH for wildland fire/atmosphere coupled simulation of the FireFlux experiment. Proc. Combust. Inst. 34, 2633–2640.
Frankman, D., Webb, B.W., Butler, B.W., Jimenez, D., Forthofer, J.M., Sopko, P., Shannon, K.S., Hiers, J.K., Ottmar, R.D., 2012. Measurements of convective and radiative heating in wildland fires. Int. J. Wildland Fire 22 (2), 157–167.
Freitas, S.R., Longo, K.M., Chatfield, R., Latham, D., Silva Dias, M.A.F., Adnreae, M.O., Prins, E., Santos, J.C., Gielow, R., Carvalho Jr., J.A., 2007. Including the sub-grid scale plume rise of vegetation fires in low resolution atmospheric transport models. Atmos. Chem. Phys. 7, 3385–3398.
Gao, W., Shaw, R.H., Paw, U.K.T., 1989. Observation of organized structure in turbulent flow within and above a forest canopy. Boundary Layer Meteorol. 47, 349–377.
Goodrick, S.L., Achtemeier, G.L., Larkin, N.K., Liu, Y., Strand, T.M., 2012. Modelling smoke transport from wildland fires: a review. Int. J. Wildland Fire 22 (1), 83–94.
Heilman, W.E., Zhong, S., Hom, J.L., Charney, J.J., Kiefer, M.T., Clark, K.L., Skowronski, N., Bohrer, G., Lu, W., Liu, Y., Kremens, R., Bian, X., Gallagher, M., Patterson, M., Nikolic, J., Chatziefstratiou, T., Stegall, C., Forbus, K., 2013. Development of modeling tools for predicting smoke dispersion from low-intensity fires. In: JFSP Project Number 09-1-04-1, pp. 61.
Heilman, W.E., Liu, Y., Urbanski, S., Kovalev, V., Mickler, R., 2014. Wildland fire emissions, carbon and climate: plume rise, atmospheric transport, and chemistry processes. For. Ecol. Manage. 317, 70–79.
Jenkins, M.A., Clark, T.L., Coen, J.L., 2001. Coupling atmospheric and fire models. In: Johnson, E.A., Miyanishi, K. (Eds.), Forest Fires: Behavior and Ecological Effects. Academic Press, San Diego, California, p. 600 pp, Chapter 7.
Kochanski, A., Jenkins, M., Mandel, J., Beezley, J., Clements, C.B., Krueger, S., 2013. Evaluation of WRF-Sfire performance with field observations from the FireFlux experiment. Geosci. Model Dev. 6, 1109–1126, http://dx.doi.org/10.5194/gmd-6-1109-2013.
Linn, R.R., Winterkamp, J.L., Weise, D.R., Edminster, C., 2010. A numerical study of slope and fuel structure effects on coupled wildfire behavior. Int. J. Wildland Fire 19, 179–201.
Mell, W.E., Manzello, S.L., Maranghides, A., Butry, D., Rehm, R.G., 2010. The wildland – urban interface fire problem – current approaches and research needs. Int. J. Wildland Fire 19, 238–251.
Morandini, F., Silvani, X., Rossi, L., Santoni, P., Simeoni, A., Balbi, J., Rossi, J.L., Marcelli, T., 2006. Fire spread experiment across Mediterranean shrub: influence of wind on flame front properties. Fire Saf. J. 41, 229–235.
Morvan, D., 2011. Physical phenomena and length scales governing the behaviour of wildfires: a case for physical modelling. Fire Technol. 47, 437–460.
Pitts, W.M., Murthy, A.V., de Ris, J.L., Filtz, J.-R., Nygard, K., Smith, D., Wetterlund, I., 2006. Round robin study of total heat flux gauge calibration at fire laboratories. Fire Saf. J. 41, 459–475.
Riggan, P.J., Tissell, R.G., Lockwood, R.N., Brass, J.A., Pereira, J.A.R., Miranda, H.S., Miranda, A.C., Campos, T., Higgins, R., 2004. Remote measurement of energy and carbon flux from wildfires in Brazil. Ecol. Appl. 14, 855–872.
Silvani, X., Morandini, F., 2009. Fire spread experiments in the field: temperature and heat fluxes measurements. Fire Saf. J. 44, 279–285.
Sofiev, M., Ermakova, T., Vankevich, R., 2012. Evaluation of the smoke-injection height from wild-land fires using remote-sensing data. Atmos. Chem. Phys. 12, 1995–2006.
Strand, T., Lamb, B., Thistle, H., Allwine, E., Peterson, H., 2009. A simple model for simulation of insect pheromone dispersion within forest canopies. Ecol. Modell. 220, 640–656.
Sullivan, A.L., Knight, I.K., 2001. Estimating error in wind speed measurements for experimental fires. Can. J. For. Res. 31 (3), 401–409.
Sun, R., Jenkins, M.A., Krueger, S.K., Mell, W., Charney, J.J., 2006. An evaluation of fire-plume properties simulated with the fire dynamics simulator (FDS) and the Clark coupled wildfire model. Can. J. For. Res. 36, 2894–2908.
Sun, R., Krueger, S.K., Jenkins, M.A., Zulauf, M.A., Charney, J.J., 2009. The importance of fire–atmosphere coupling and boundary-layer turbulence to wildfire spread. Int. J. Wildland Fire 18, 50–60.
Taylor, S.W., Wotton, B.M., Alexander, M.E., Dalrymple, G.N., 2004. Variation in wind and crown fire behavior in a northern jack pine–black spruce forest. Can. J. For. Res. 34, 1561–1576.
Vickers, D., Mahrt, L., 1997. Quality control and flux sampling problems for tower and aircraft data. J. Atmos. Ocean. Technol. 14, 512–526.
Wilczak, J.M., Oncley, S.P., Stage, S.A., 2001. Sonic anemometer tilt correction algorithms. Boundary Layer Meteorol. 99, 127–150.